

Enabling Mitochondrial Uptake of Lipophilic Dications Using Methylated Triphenylphosphonium Moieties

How Chee Ong,^{†,#} Zhang Hu,^{†,#} João T. S. Coimbra,^{‡,ic} Maria J. Ramos,^{‡,ic} Oi Lian Kon,[§] Bengang Xing,^{†,ic} Edwin K. L. Yeow,^{†,ic} Pedro A. Fernandes,^{*,‡} and Felipe García^{*,†,ic}

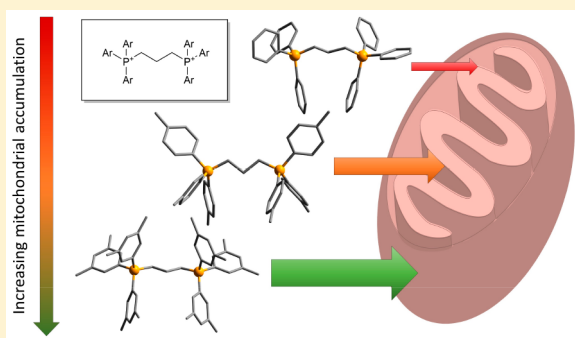
[†]School of Physical and Mathematical Sciences, Division of Chemistry and Biological Chemistry, Nanyang Technological University, 21 Nanyang Link, 637371, Singapore

[‡]UCIBIO, REQUIMTE, Departamento de Química e Bioquímica, Faculdade de Ciências, Universidade do Porto, Rua do Campo Alegre s/n, 4169-007, Porto, Portugal

[§]Division of Medical Sciences, Laboratory of Applied Human Genetics, Humphrey Oei Institute of Cancer Research, National Cancer Centre, 169610, Singapore

Supporting Information

ABSTRACT: Triphenylphosphonium (TPP⁺) species comprising multiple charges, i.e., bis-TPP⁺, are predicted to be superior mitochondrial-targeting vectors and are expected to have mitochondrial accumulations 1000-fold greater than TPP⁺, the current “gold standard”. However, bis-TPP⁺ vectors linked by short hydrocarbon chains ($n < 5$) are unable to be taken up by the mitochondria, thus hindering their development as mitochondrial delivery vectors. Through the incorporation of methylated TPP⁺ moieties (T*PP⁺), we successfully enabled the accumulation of bis-TPP⁺ with a short linker chain in isolated mitochondria, as measured by high performance liquid chromatography. These experimental results are further supported by molecular dynamics and ab initio calculations, revealing the strong correlations between mitochondria uptake and molecular volume, surface area, and chemical hardness. Most notably, the molecular volume has been shown to be a strong predictor of accumulation for both mono- and bis-TPP⁺ salts. Our study underscores the potential of T*PP⁺ moieties as alternative mitochondrial vectors to overcome low permeation into the mitochondria.



INTRODUCTION

Mitochondria organelle are well-known for their pivotal role in aerobic respiration¹ and other essential cellular functions, such as cell signaling^{2,3} and apoptosis.⁴ Furthermore, aberrant mitochondria has been linked to many neurodegenerative and cardiovascular diseases such as Alzheimer’s disease, atherosclerosis, amyotrophic lateral sclerosis (ALS), and cancer.^{5–9} Hence, as mitochondria is increasingly recognized to play a critical role in human disease, it is vital to develop more efficient vectors that selectively target mitochondria.

Typically, mitochondrial targeting vectors are positively charged species that selectively accumulate within the organelle due to the large negative membrane potential across the inner mitochondrial membrane ($\Delta\psi = -150$ – 180 mV).⁴ Common examples include rhodamines, cyanines, mitochondrion-targeting peptides, and triphenylphosphonium (TPP⁺) salts.^{10–13} The most extensively studied, “gold standard” vector, TPP⁺, boasts ease of synthesis, stability in biological systems, and facile conjugation to molecular cargo, and has been used to successfully deliver a wide range of molecular cargo into mitochondria.^{14–19}

The uptake of TPP⁺ by the mitochondrion is modeled by the Nernst equation,^{10,20} which predicts the equilibrium concentration of bis-TPP⁺ to be 1000-fold greater than mono-TPP⁺ (-180 mV), thus suggesting enhanced mitochondrial targeting properties.²¹ In addition, although mono-TPP⁺ can show selectivity between cancer and noncancer cells,^{22,23} bis-TPP⁺ species are more sensitive to small changes in membrane potentials, which may confer enhanced selectivity.²⁴ For instance, cancerous cells display higher $|\Delta\psi|$ (ca. 60 mV) than normal cells, which corresponds to a 10-fold increase in selectivity (relative to mono-TPP⁺) according to the Nernst equation.^{25,26} However, an increased cationic charge elevates the kinetic barrier for the transport of bis-TPP⁺ across phospholipid bilayers,^{27,28} a principle corroborated by the work by Murphy et al., who demonstrated that incorporation of methylene bridges comprising less than five carbon atoms resulted in the unsuccessful mitochondrial uptake of bis-TPP⁺ (Figure 1).²¹

Received: December 14, 2018

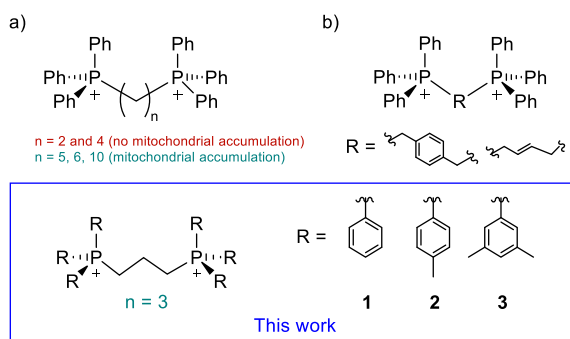


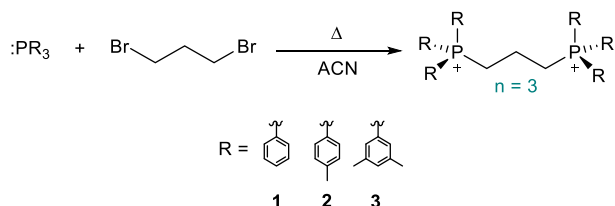
Figure 1. Previously reported bis-TPP⁺ cations: (top) Murphy et al.²¹ and (bottom) Lisanti et al.³⁵

In light of the apparent inability of bis-TPP⁺ salts linked by short methylene linkers ($n \leq 5$) to accumulate, we set out to study the effect of T*PP⁺ moieties²⁸ on the mitochondrial uptake of short-chained bis-TPP⁺ dicationic species. In stark contrast with their previously reported TPP counterparts, we report the successful accumulation of dicationic bis-T*PP⁺ species containing short linker chains. This work demonstrates that the use of T*PP⁺ moieties allows for the rational fine-tuning of steric and electronic parameters toward their accumulation in mitochondria and represents a straightforward strategy to readily enhance mitochondrial uptake of dicationic species.

RESULTS AND DISCUSSION

Synthesis and Structure of Compounds 1–3. In our study, we based the initial choice of phosphine starting materials on previously reported work, where T*PP⁺ mitochondrial delivery vectors comprising *p*-tolyl or 3,5-dimethylphenyl trisubstituted phosphonium moieties significantly increase the accumulation of both the T*PP⁺ cations and their conjugated cargo into the mitochondria organelle.²⁹ Dications 1–3 were obtained in quantitative spectroscopic yield upon reacting the respective phosphines with 1,3-dibromopropane in acetonitrile under reflux (Scheme 1).

Scheme 1. Synthesis of Bis-TPP⁺ and Bis-T*PP⁺ salts 1–3



In agreement with previous observations for monocationic T*PP⁺ species,²⁹ attempts to obtain dicationic species with more heavily substituted phosphines, such as trimesitylphosphine, were unsuccessful. Compounds 1–3 were purified by

crystallization in a mixture of acetonitrile and diethyl ether (isolated crystalline product yields between 65 and 70%).

Nuclear magnetic resonance (NMR) spectroscopic analysis reveals the successful formation of the phosphonium salts, as shown by the characteristic downfield shifts relative to the free phosphine in the ³¹P{¹H} NMR spectra (−5.4, −7.9, −5.8 ppm^{30,31} vs 25.2, 24.0, and 24.6 ppm for 1–3 respectively), consistent with the chemical shifts reported in the literature.^{21,29} The ¹³C{¹H} NMR spectra confirms the successful linkage of two phosphonium moieties on the same molecule, as seen from the ABX splitting patterns observed (C_{ortho}, C_{meta}, and P–C_{alkyl}) as a result of second-order spin coupling.

The single-crystal structural data show that the P–C_{Ar} bond lengths ranges from 1.789–1.802 Å, 1.785–1.801 Å, and 1.790–1.806 Å, while the P–C_{alkyl} ranges from 1.796–1.801 Å, 1.792–1.793 Å and 1.789–1.804 Å for compounds 1, 2, and 3 respectively. This is highly consistent with the bond lengths expected of alkyltriarylphosphonium P–C bonds at 1.796 (±0.017) Å for P–C_{Ar} and 1.798 (±0.031) Å for P–C_{alkyl}.³² The bond angles for C–P–C bonds for all three compounds ranges from 105.10 to 113.56°, which is consistent with a tetrahedral geometry expected of phosphonium moieties.³³

Partition Coefficient and Mitochondrial Uptake of Compounds 1–3. The octanol–water partition coefficients (P) for compounds 1–3 (i.e., ratio of the concentration of dication in 1-octanol to the concentration of dication in water) were determined to establish their relative lipophilicities (Table 1), which has been shown to influence membrane permeability.³⁴ The observed trend indicates that the bis-T*PP⁺ dication 3, containing dimethyl substituted phenyl rings, has the greatest lipophilicity, followed by methyl substituted dication 2 and last compound 1, which comprises TPP⁺ moieties (Table 1 and Figure 3).

In order to evaluate if the hydrophobic variation observed for 1–3 is translated to differences in half-maximal inhibitory concentrations (IC₅₀), their 72-h IC₅₀ values in HeLa cells were determined. It was observed that with an increasing degree of methylation, the IC₅₀ decreased from 180 μM to 21 μM and 6 μM for 1 to 3, respectively, suggesting increasing mitochondrial accumulation with increasing degree of substitution—consistent with their monocationic counterparts.²⁹ Moreover, a reduction in IC₅₀ values for mono- and dicationic TPP⁺ species has been recently linked to reduced ATP levels (i.e., suggestive of increased mitochondrial accumulation) in studies proposing the use of TPP⁺ and bis-TPP⁺ cations as a novel strategy toward the selective eradication of cancer stem cells (CSCs).³⁵

To rule out any differences in intrinsic toxicity between the dications 1–3—and to further corroborate if the variation in IC₅₀ values was caused by enhanced mitochondrial uptake—the accumulation in isolated mitochondria (C_m) was established (see Supporting Information).

The trend of C_m values obtained shows a significant improvement in the rate of uptake with increasing methylation,

Table 1. Summary of Experimental and Computational Results for Compounds 1, 2, and 3

compound	log P	IC ₅₀ /μM	C _m /mmol g ⁻¹	volume/Å ³	SASA/Å ²	ΔG _{aq→oct} ^{exp} /kcal mol ⁻¹	ΔΔG _{aq→oct} ^{vdW} /kcal mol ⁻¹	η/eV
2	−0.12 ± 0.03	21.3 ± 1.6	5.2 ± 0.4	1862.7 ± 1.5	1014.5 ± 1.0	0.16 ± 0.04	−5.56 ± 0.30	3.65
1	−1.62 ± 0.13	181.3 ± 7.6	0.0	1570.9 ± 1.1	860.3 ± 0.8	2.21 ± 0.18	0.00 ± 0.35	3.79
3	0.70 ± 0.08	5.6 ± 0.3	20.3 ± 1.2	2120.0 ± 1.6	1108.9 ± 1.0	−0.95 ± 0.11	−7.94 ± 0.45	3.52

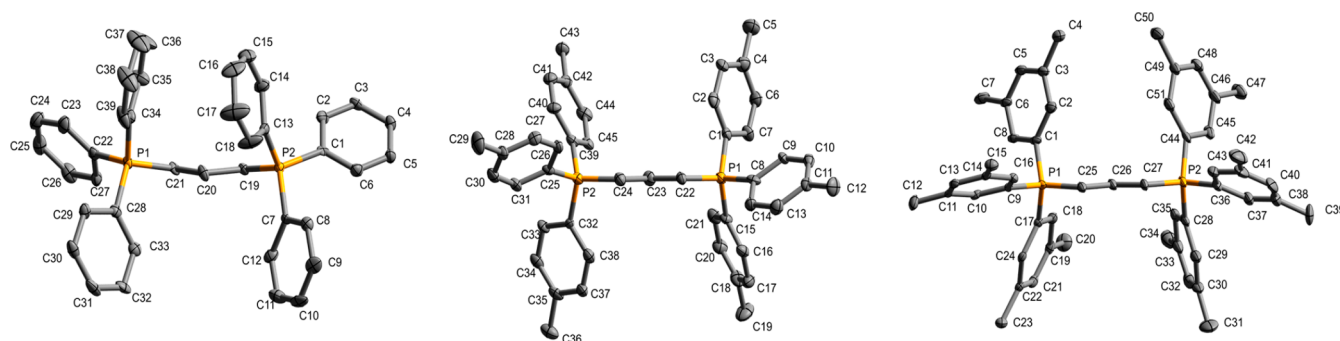


Figure 2. Selected bond lengths (Å) and angles (deg) of compound 1 C21–P1 1.800(6) C22–P1 1.798(6) C21–P1–C22 110.8(3) C22–P1–C28 108.9(3); Compound 2 C22–P1 1.789(10) C1–P1 1.799(10) C1–P1–C22 110.9(5) C1–P1–C8 107.0(4); Compound 3 C25–P1 1.793(4) C1–P1 1.800(8) C1–P1–C25 113.6(5) C1–P1–C9 105.2(7). Thermal ellipsoids are shown at the 50% probability level. Hydrogen atoms and bromide anions have been omitted for clarity.

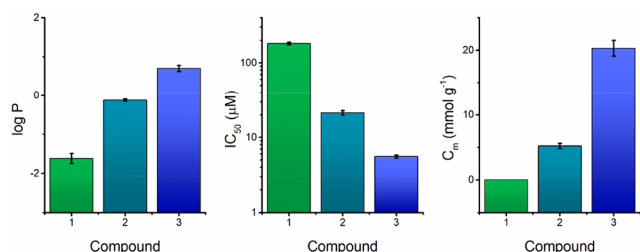


Figure 3. Experimental results obtained for log P, IC₅₀, and C_m. Error bars (±) refer to the standard deviation (SD).

from negligible uptake of **1** to 5.2 mmol g⁻¹ and 20.3 mmol g⁻¹ in **2** and **3**, respectively. The negligible accumulation of compound **1** is in agreement with reports by Murphy et al. (vide supra).²¹ The experimental trend suggests that the increased IC₅₀ values is not due to the intrinsic cytotoxicity of the compounds but is rather due to its enhanced accumulation within the HeLa cells.

Furthermore, the supernatant concentration of compound **3**—the most accumulating compound presented in our study—was measured using HPLC after treatment of the mitochondria with carbonyl cyanide *p*-trifluoromethoxyphenylhydrazone (FCCP), to abolish the membrane potential across the mitochondrial membrane, resulting in the efflux of compound **3** (see Supporting Information). This indicates that **3** does not accumulate in the mitochondria when Δψ is abolished, and the accumulation of **3** is thus driven by the presence of the membrane potential.

THEORETICAL STUDIES

To better understand the mechanism underlying the observed increase in mitochondrial uptake, we considered the corresponding membrane transport kinetics. The kinetic barrier for the permeation of small charged molecules across a phospholipid membrane in an aqueous environment can be approximated by the free energy of transport from the aqueous phase into the center of the lipid membrane,³⁶ and is hence closely linked to lipophilicity.²¹ This barrier mainly comprises the Born and hydrophobic (or neutral) free energies,^{28,37} which can be treated as two independent components.^{34,38}

The Born free energy, $W_B = 339(Z^2/r)$, the most significant electronic component of this kinetic barrier, is directly proportional to the square of the ionic charge (Z), and inversely proportional to the ionic radius (r) for a spherical ion, whereas the hydrophobic free energy was empirically

found to be proportional to the accessible surface area of the cation (r^2).^{28,37}

Although the ionic radius is commonly used to calculate the Born and hydrophobic free energy, compounds **1–3** are far from spherical. Hence, using an average radius to calculate the kinetic barrier of transport for a nonspherical ion might render the results obtained inaccurate. Moreover, previous reports of substituted TPP⁺ moieties as mitochondrial delivery agents were mostly limited to biological activity quantification, while the ones describing structural correlation with accumulation did not consider nonspherical effects.^{35,39–42}

Solvent Accessible Surface Area (SASA) and Molecular Volume (V). For this purpose, molecular dynamics (MD) calculations were carried out (see Supporting Information) to determine the impact of methylation on the volume (V) and solvent accessible surface area (SASA) as an alternative parameter to molecular radius. MD simulations revealed that as the number of methyl groups increases, a larger (hydrophobic) volume (and SASA) is accessible to the solvent decreasing the polar interactions with the molecules of water, resulting in an increasingly poorer cation solvation. On the other hand, the larger nonpolar volume enhances the level of nonpolar interactions leading to a favorable partition into the organic solvent (i.e., more negative $\Delta G_{aq \rightarrow oct}$), as seen from the strong linear correlation ($r^2 = 0.986$ and 0.999) for V and SASA, respectively (See Figure 4).

While the relationship between mitochondrial accumulation and nonpolar molecular SASA has been experimentally established in T*PP⁺ compounds,²⁹ and is also reflected in the case of bis-T*PP⁺ molecules, the strong correlation observed between molecular volume (whose surrogates are surface and radius) and mitochondrial accumulation has never been described. Furthermore, the importance of molecular volume as a meaningful parameter to predict mitochondrial accumulation for multiply charged TPP⁺ species will be discussed further in the text (vide infra).

Neutral and Electrostatic Components for the Free Energy of Transfer. Thermodynamic integration (TI) calculations were used to quantify the nonpolar component (i.e., vdW) of the relative free energy of transfer of compounds **1–3** from water to 1-octanol ($\Delta\Delta G_{aq \rightarrow oct}^{vdw}$) taking compound **1** as the reference (Table 1). Similar to previous reports on monocationic species, initial TI results showed that the electrostatic component (i.e., Born component) of compounds **1–3** showed negligible variation (see Supporting Information for details).²⁹ Thus, the results presented were obtained by

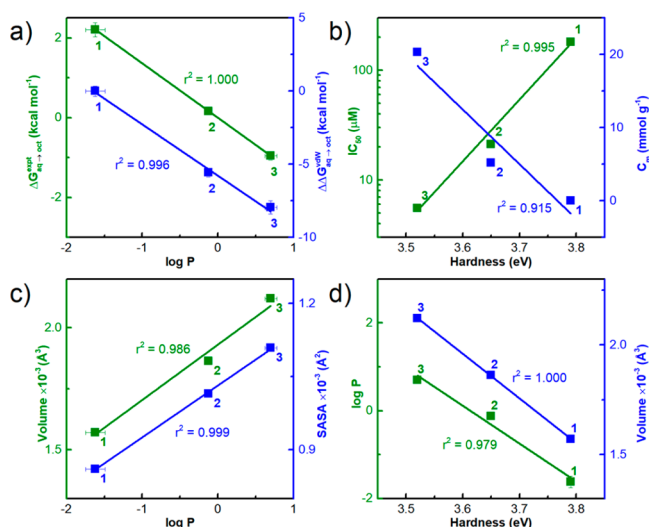


Figure 4. Correlation graphs between (a) $\Delta G_{\text{aq} \rightarrow \text{oct}}^{\text{expt}}$ and $\Delta \Delta G_{\text{aq} \rightarrow \text{oct}}^{\text{vdw}}$ against $\log P$ (b) IC_{50} and C_m against hardness, (c) volume and SASA against $\log P$, (d) $\log P$ and volume against hardness. Error bars (\pm) refers to the standard deviation (SD).

considering only the nonelectrostatic components. The results show a strong negative correlation between $\Delta \Delta G_{\text{aq} \rightarrow \text{oct}}^{\text{vdw}}$ and the mitochondrial uptake, with decreasing free energy of transport from compounds 1 to 3 (0.00, -5.56 , and -7.94 kcal mol $^{-1}$, respectively).

The thermodynamic integration calculations trends were consistent with the $\Delta G_{\text{aq} \rightarrow \text{oct}}^{\text{exp}}$ calculated from $\log P$ ($\Delta G = -2.303 RT \log P$) (Figure 4 and Table 1). The calculated decrease in kinetic barrier to permeate the membrane can be attributed to the increased number of nonpolar substituents present on bis-T*PP $^+$ species (i.e., 2 and 3) as compared to bis-T*PP $^+$. This increased affinity of the bis-T*PP $^+$ for the hydrophobic phase lowers the permeation energy barrier resulting in greater mitochondrial uptake, which is in agreement with our experimentally observed C_m and IC_{50} values. Taken together, these findings suggest that the use of T*PP $^+$ moieties—with varying levels of substitution—is a highly effective approach to improving the effectiveness of bis-T*PP $^+$ species as mitochondrial vectors.

Electrostatic Potential and Chemical Hardness for Compounds 1–3 and Previously Reported Dications.

To examine the changes in the electronic interactions due to methylation, density functional theory (DFT) calculations (B3LYP/6-31+G(d)) were performed, determining the electrostatic potential (ESP) maps and chemical hardness of 1–3. Electrostatic potential maps depict the local electron density distribution, serving as a measure of the available polar surface area for polar interactions,¹⁴ and it has been observed from works of Murphy²¹ and Hartley¹⁴ that a reduction in the electrostatic potential in cationic species can be correlated with an increase in membrane permeation.

The chemical hardness serves as an indicator of electron cloud polarizability, and the strength of hydrophobic interactions,⁴³ and was obtained for 1–3 from the vertical ionization potentials (IP) and electron affinities (EA), calculated at the B3LYP/6-311+G(2df,p) level, with the following expression: $\eta = (IP - EA)/2$ (see Table 2). We herein utilize these parameters as intrinsic molecular descriptors to correlate and further our basic understanding of the electronic

Table 2. Vertical Ionization Energy (IP), Electron Affinity (EA), and Hardness Values for the Three Bis-T*PP $^+$ Cations in This Work (Cations 1, 2, and 3) and for the Previously Reported Bis-T*PP $^+$ Cations by Murphy et al. (PC2P, PC4P, PC5P, PC6P, and PC10P)^a

cation	IP/eV	EA/eV	hardness/eV
PC2P	13.45	5.85	3.80
1	13.20	5.63	3.79
PC4P	12.98	5.40	3.79
PC5P	12.81	5.24	3.78
PC6P	12.64	5.11	3.76
2	12.58	5.29	3.65
PC10P	12.15	4.78	3.69
3	12.25	5.20	3.52

^aFor the bis-T*PP $^+$ cations proposed by Murphy et al., we have used the same nomenclature as in the original work. Compounds are ordered in increasing molecular weight.

properties of 1–3 in relation to their mitochondrial uptake trends.

The ESP maps (see Figure 5) revealed that the electron density located in the volume between the two P $^+$ atoms increases with increased substitution. The presence of electron-donating methyl groups increasingly promotes the dissipation of the positive charge across the molecule from 1 to 3 and renders the methylated compounds more lipophilic in nature. This agrees with the calculated chemical hardness values, which decrease from 3.79, 3.65, to 3.52 eV in 1–3, respectively. Chemical hardness is negatively correlated with the mitochondrial uptake, indicating that softening the phosphonium cation improves the membrane permeability—and hence the mitochondrial accumulation.

The same phenomenon could also be observed from bis-T*PP $^+$ previously investigated by Murphy and co-workers.²¹ Further calculations revealed that the increase of the alkyl chain length was also accompanied by a decrease in chemical hardness (see Table 2) and lipophilicity.²¹ Furthermore, it can be observed from the calculated value for all eight dications that the chemical hardness decreased with increasing molecular weight. However, dication 2 displays a lower chemical hardness than PC $_{10}$ P, which comprises one additional carbon atom—suggesting methyl substitution as a more effective approach to dissipating the positive charge on this species than the commonly used chain extension approach.

These results therefore suggest that lipophilicity may be tunable and improved from structural modifications targeted to reducing charge density as well as the HOMO–LUMO gap for T*PP $^+$ compounds.

Unifying Mono-T*PP $^+$ and Bis-T*PP $^+$ Accumulation: Volume Per Charge Unit (V_{PC}).

Comparison between the previously reported mono-T*PP $^+$ ²⁹ and bis-T*PP $^+$ 1–3 species revealed that the correlation between accumulation of TPP $^+$ salts and lipophilicity was not satisfactory. Although the trends between accumulation and lipophilicity are internally consistent within each type of TPP $^+$ salts (mono- or bis-T*PP $^+$), the linear correlation cannot be generalized to both (Figure 6a). To bridge the gap between the differing accumulations in mono and bis-T*PP $^+$, we investigated the new structural parameters described above ($V/SASA/\eta$) and their correlation with C_m . As η correlates well with $\log P$ (Figure 4d), two separate trendlines (similar to the correlation with $\log P$) were observed. Thus, a satisfactory correlation

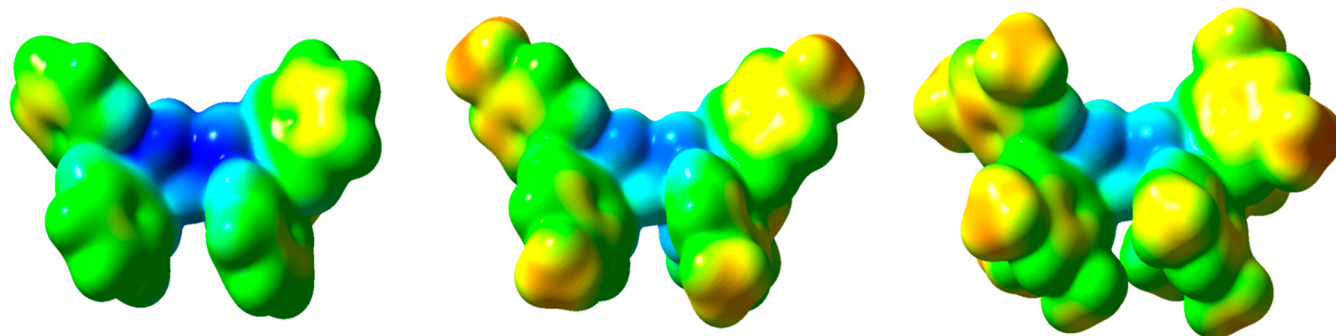


Figure 5. ESP maps (B3LYP/6-31G(d)) for compounds **1**, **2**, and **3**. Regions with high electron density (less positive electrostatic potential) are colored red, and regions with low electron density (more positive electrostatic potentials) are colored blue. Yellow and green correspond to intermediate electrostatic potentials. The same color scale was used: from 0.115 (red) to 0.238 au (dark blue). An isodensity value of 0.0020 e a₀⁻³ was used to define the outer surface of the molecules on which the ESP was calculated.

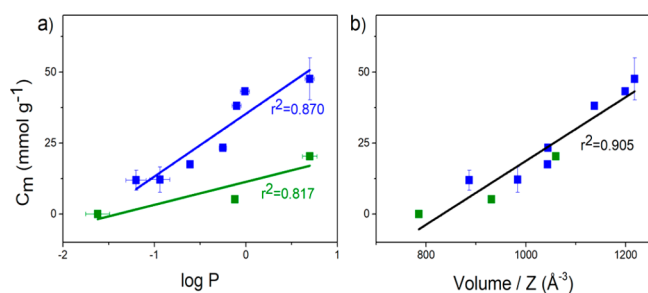


Figure 6. Correlations plots between (a) C_m against $\log P$ and (b) C_m against volume/charge for mono- and bis-T*PP⁺. Error bars correspond to the SD. Mono- and bis-T*PP⁺ are colored blue and green, respectively.

between mono- and bis-T*PP⁺ was not possible (see Supporting Information, Figure S4).

Notably, the molecular volume, on the other hand, upon normalization with respect to charge (V/Z)—volume per charge (V_{PC})—provided a generalizable linear correlation (Figure 6b). Although the volume and SASA follows the same general trend, we focused on volume due to the slightly higher r^2 values. The experimentally obtained equation— $V_{PC} = 8.06^*C_m + 852$ —underscores a strong relationship between the mitochondrial accumulation of T*PP⁺ species and their V_{PC} . Furthermore, the data obtained suggests the existence of a minimum V_{PC} (V_{PC}^{\min}) threshold of 852 Å³ required for the effective permeation of T*PP⁺ species into mitochondria organelle.

To further assess the validity of the obtained equation, the volume and SASA of compounds studied by Murphy et al. (i.e., PC₂P, PC₄P, PC₃P, PC₆P, PC₁₀P) were calculated and compared with the values obtained for compounds **1–3** (see Table 3). From the experimentally obtained equation, the minimum permeation volume (V_{PC}^{\min}) required for a bis-T*PP⁺ is calculated to be 1704 Å³. Thus, it is predicted that PC₄P ($V = 1650.9$ Å³) would not accumulate in the mitochondria, while PC₃P ($V = 1708.4$ Å³) would be able to do so. This is consistent with their previously reported experimental results,²¹ demonstrating that the herein reported methodology is robust. However, it should be noted that this relationship may not hold if the molecular structure varies significantly from that of TPP⁺ salts presented in this work. Overall, these findings suggest that the volume parameter could be useful for the prediction of mitochondrial accumulation, especially for multivalent TPP⁺ compounds.

Table 3. Solvent Accessible Surface Area (SASA) and Volume (V) Computational Results for Compounds **1–3** and the Previously Reported Bis-T*PP⁺ Cations by Murphy et al. (PC₂P, PC₄P, PC₃P, PC₆P, and PC₁₀P) in water^a

cation	SASA/Å ²	V/Å ³	mitochondrial accumulation
PC ₂ P	855.0 ± 0.8	1534.2 ± 1.1	NO
1	860.3 ± 0.8	1570.9 ± 1.1	NO
PC ₄ P	932.6 ± 1.1	1650.9 ± 1.2	NO
PC ₃ P	968.4 ± 1.0	1708.4 ± 1.2	YES
PC ₆ P	985.0 ± 1.3	1750.9 ± 1.5	YES
2	1014.5 ± 1.0	1862.7 ± 1.5	YES
PC ₁₀ P	1110.0 ± 1.3	1964.3 ± 1.6	YES
3	1108.9 ± 1.0	2120.0 ± 1.0	YES

^aFor the bis-T*PP⁺ cations proposed by Murphy et al., we have used the same nomenclature as in the original work.

Quantitative Structure–Activity Relationship (QSAR) Models. In order to confirm that the mitochondrial uptake is consistent with the current QSAR models, we considered the model developed by Horobin et al.,^{44–46} which relates physicochemical parameters of compounds to the intracellular localization. These parameters are used to determine the subcellular localization of compounds and thus can be used to predict whether the compounds will be mitochondria-targeting. For mitochondrial localization, the model considers the following parameters: amphiphilic index (AI), conjugated bond number (CBN), $\log P$, pK_a , and electric charge (Z). For compounds **1–3**, the pK_a and AI are not considered due to a lack of acidic protons and amphiphilicity. As such, for selective mitochondria accumulation, the relevant criteria for compounds **1–3** to satisfy are $CBN < 40$, $5 > \log P > 0$, $Z > 0$.

From the structures of compounds **1–3**, the key determining factor for mitochondria targeting lies with the $\log P$ value. All three compounds have an identical CBN and Z value, and they satisfy the criteria for CBN and Z as previously described ($CBN = 18$, $Z = 2$). For the lipophilicity, compound **1** falls far below the $\log P$ requirement with a $\log P$ of -1.62 , resulting in negligible mitochondrial accumulation, as predicted by the QSAR model. Compound **3**, on the other hand, had a $\log P$ of 0.70, which fell within the range of $0 < \log P < 5$, which resulted in a high mitochondrial accumulation. Compound **2** had a $\log P$ of -0.12 , which was slightly lower than the lower limit, resulting in a poor mitochondrial uptake, as reflected by its C_m value. The uptake observed for the

compounds studied thus conforms well and is consistent with current QSAR models.

This model shows that bis-TPP⁺ linked by short chains do possess the necessary characteristics for mitochondrial accumulation. However, these systems can be limited by the lipophilicity, as corroborated by both the QSAR model, as well as the C_m values for compounds 1–3. This further supports the strategy of phenyl methylation, as it can be used to overcome this logP limitation by boosting the logP into the optimal range, thus enabling more efficient accumulation within the mitochondria.

CONCLUSIONS

In summary, we report the use of T*PP⁺ moieties to address the inability of TPP⁺ dications comprising short chain linkers to be taken up by the mitochondria organelle. The incorporation of nonpolar methyl groups increases the volume and SASA of the resulting bis-T*PP⁺ salts—while dispersing their high charge density and decreasing their chemical hardness—which in turn enhances their lipophilicity and mitochondrial accumulation. Furthermore, ESP maps and chemical hardness calculations could serve as useful tools to predict the efficacy of TPP⁺ mitochondrial vectors in silico. These results demonstrate that substituents on the phenyl rings increase the volume and that mitochondrial accumulation can be readily enhanced by fine-tuning these properties through structural modifications. In particular, molecular volume has been shown to be a key parameter for the prediction of compounds incorporating multiple TPP⁺ moieties. From our observations across various mono- and bis-TPP⁺, we propose the minimum permeation volume per charge (V_{PC}^{min}), which can be used as a new structural parameter for the prediction of mitochondrial accumulation for TPP⁺ molecules.

Our work not only highlights the use of readily tunable molecular descriptors as key parameters to design future TPP⁺ mitochondrial delivery vectors with enhanced properties, thereby enhancing bioavailability of TPP⁺-conjugated drugs, but also illustrates the need for a broader family of T*PP⁺ species for future enhanced mitochondrial therapies.

ASSOCIATED CONTENT

Supporting Information

The Supporting Information is available free of charge on the ACS Publications website at DOI: 10.1021/acs.inorgchem.8b03380.

Experimental procedures, details for MD and DFT calculations, NMR/HRMS spectra for compounds 1–3 (PDF)

Accession Codes

CCDC 1478287–1478289 contain the supplementary crystallographic data for this paper. These data can be obtained free of charge via www.ccdc.cam.ac.uk/data_request/cif, or by emailing data_request@ccdc.cam.ac.uk, or by contacting The Cambridge Crystallographic Data Centre, 12 Union Road, Cambridge CB2 1EZ, UK; fax: +44 1223 336033.

AUTHOR INFORMATION

Corresponding Authors

*(F.G.) E-mail: fgarcia@ntu.edu.sg.

*(P.A.F.) E-mail: paferman@fc.up.pt.

ORCID

João T. S. Coimbra: 0000-0001-9138-7498

Maria J. Ramos: 0000-0002-7554-8324

Bengang Xing: 0000-0002-8391-1234

Edwin K. L. Yeow: 0000-0003-0290-4882

Felipe García: 0000-0002-9605-3611

Author Contributions

#H.C.O. and Z.H. contributed equally.

Notes

The authors declare no competing financial interest.

ACKNOWLEDGMENTS

F.G. would like to thank A*STAR AME IRG A1783c0003, NTU for a start-up grant (M4080552) and MOE Tier 1 grants (RG 11/15 and RG 113/16) for financial support. P.A.F., M.J.R., and J.T.S.C. acknowledge financial support from the European Union (FEDER funds POCI/01/0145/FEDER/007728) and National Funds (FCT/MEC, Fundação para a Ciência e Tecnologia and Ministério da Educação e Ciência) under the Partnership Agreement PT2020 UID/MULTI/04378/2013.

REFERENCES

- (1) Kuhlbrandt, W. Structure and function of mitochondrial membrane protein complexes. *BMC Biol.* **2015**, *13*, 89–99.
- (2) Rizzuto, R.; De Stefani, D.; Raffaello, A.; Mammucari, C. Mitochondria as sensors and regulators of calcium signalling. *Nat. Rev. Mol. Cell Biol.* **2012**, *13* (9), 566–578.
- (3) Chandel, N. S. Mitochondria as signaling organelles. *BMC Biol.* **2014**, *12* (1), 34–40.
- (4) Murphy, M. P.; Smith, R. A. Drug delivery to mitochondria: the key to mitochondrial medicine. *Adv. Drug Delivery Rev.* **2000**, *41* (2), 235–250.
- (5) Di Lisa, F.; Kaludercic, N.; Carpi, A.; Menabo, R.; Giorgio, M. Mitochondria and vascular pathology. *Pharmacol. Rep.* **2009**, *61* (1), 123–130.
- (6) Frantz, M. C.; Wipf, P. Mitochondria as a target in treatment. *Environ. Mol. Mutagen.* **2010**, *51* (5), 462–475.
- (7) Reddy, P. H. Mitochondrial medicine for aging and neurodegenerative diseases. *NeuroMol. Med.* **2008**, *10* (4), 291–315.
- (8) Celsi, F.; Pizzo, P.; Brini, M.; Leo, S.; Fotino, C.; Pinton, P.; Rizzuto, R. Mitochondria, calcium and cell death: a deadly triad in neurodegeneration. *Biochim. Biophys. Acta, Bioenerg.* **2009**, *1787* (5), 335–344.
- (9) Haelterman, N. A.; Yoon, W. H.; Sandoval, H.; Jaiswal, M.; Shulman, J. M.; Bellen, H. J. A mitocentric view of Parkinson's disease. *Annu. Rev. Neurosci.* **2014**, *37* (1), 137–159.
- (10) Zielonka, J.; Joseph, J.; Sikora, A.; Hardy, M. O.; Ouari, O.; Vasquez-Vivar, J.; Cheng, G.; Lopez, M.; Kalyanaraman, B. Mitochondria-Targeted Triphenylphosphonium-Based Compounds: Syntheses, Mechanisms of Action, and Therapeutic and Diagnostic Applications. *Chem. Rev.* **2017**, *117* (15), 10043–10120.
- (11) Johnson, L. V.; Walsh, M. L.; Chen, L. B. Localization of mitochondria in living cells with rhodamine 123. *Proc. Natl. Acad. Sci. U. S. A.* **1980**, *77* (2), 990–994.
- (12) Laris, P. C.; Bahr, D. P.; Chaffee, R. R. J. Membrane-Potentials in Mitochondrial Preparations as Measured by Means of a Cyanine Dye. *Biochim. Biophys. Acta, Bioenerg.* **1975**, *376* (3), 415–425.
- (13) Szeto, H. H. Cell-permeable, mitochondrial-targeted, peptide antioxidants. *AAPS J.* **2006**, *8* (2), E277–E283.
- (14) Robb, E. L.; Gawel, J. M.; Aksentijevic, D.; Cocheme, H. M.; Stewart, T. S.; Shchepinova, M. M.; Qiang, H.; Prime, T. A.; Bright, T. P.; James, A. M.; Shattock, M. J.; Senn, H. M.; Hartley, R. C.; Murphy, M. P. Selective superoxide generation within mitochondria by the targeted redox cycler MitoParaquat. *Free Radical Biol. Med.* **2015**, *89*, 883–894.

- (15) Jameson, V. J.; Cocheme, H. M.; Logan, A.; Hanton, L. R.; Smith, R. A.; Murphy, M. P. Synthesis of triphenylphosphonium vitamin E derivatives as mitochondria-targeted antioxidants. *Tetrahedron* **2015**, *71* (44), 8444–8453.
- (16) Millard, M.; Gallagher, J. D.; Olenyuk, B. Z.; Neamati, N. A selective mitochondrial-targeted chlorambucil with remarkable cytotoxicity in breast and pancreatic cancers. *J. Med. Chem.* **2013**, *56* (22), 9170–9179.
- (17) Finichiu, P. G.; Larsen, D. S.; Evans, C.; Larsen, L.; Bright, T. P.; Robb, E. L.; Trnka, J.; Prime, T. A.; James, A. M.; Smith, R. A.; Murphy, M. P. A mitochondria-targeted derivative of ascorbate: MitoC. *Free Radical Biol. Med.* **2015**, *89*, 668–678.
- (18) Kelso, G. F.; Porteous, C. M.; Coulter, C. V.; Hughes, G.; Porteous, W. K.; Ledgerwood, E. C.; Smith, R. A.; Murphy, M. P. Selective targeting of a redox-active ubiquinone to mitochondria within cells: antioxidant and antiapoptotic properties. *J. Biol. Chem.* **2001**, *276* (7), 4588–4596.
- (19) Kaur, A.; Brigden, K. W. L.; Cashman, T. F.; Fraser, S. T.; New, E. J. Mitochondrially targeted redox probe reveals the variations in oxidative capacity of the haematopoietic cells. *Org. Biomol. Chem.* **2015**, *13* (24), 6686–6689.
- (20) Murphy, M. P.; Smith, R. A. Targeting antioxidants to mitochondria by conjugation to lipophilic cations. *Annu. Rev. Pharmacol. Toxicol.* **2007**, *47*, 629–656.
- (21) Ross, M. F.; Da Ros, T.; Blaikie, F. H.; Prime, T. A.; Porteous, C. M.; Severina, I. I.; Skulachev, V. P.; Kjaergaard, H. G.; Smith, R. A.; Murphy, M. P. Accumulation of lipophilic dicationic agents in mitochondria and cells. *Biochem. J.* **2006**, *400* (1), 199–208.
- (22) Morrison, D. E.; Aitken, J. B.; de Jonge, M. D.; Issa, F.; Harris, H. H.; Rendina, L. M. Synthesis and Biological Evaluation of a Class of Mitochondrially-Targeted Gadolinium(III) Agents. *Chem. - Eur. J.* **2014**, *20* (50), 16602–16612.
- (23) Ucar, E.; Seven, O.; Lee, D.; Kim, G.; Yoon, J.; Akkaya, E. U. Selectivity in Photodynamic Action: Higher Activity of Mitochondria Targeting Photosensitizers in Cancer Cells. *ChemPhotoChem* **2019**, *3* (3), 129–132, DOI: 10.1002/cptc.201800231.
- (24) Logan, A.; Pell, V. R.; Shaffer, K. J.; Evans, C.; Stanley, N. J.; Robb, E. L.; Prime, T. A.; Chouchani, E. T.; Cocheme, H. M.; Fearnley, I. M.; Vidoni, S.; James, A. M.; Porteous, C. M.; Partridge, L.; Krieg, T.; Smith, R. A.; Murphy, M. P. Assessing the Mitochondrial Membrane Potential in Cells and In Vivo using Targeted Click Chemistry and Mass Spectrometry. *Cell Metab.* **2016**, *23* (2), 379–385.
- (25) Hu, Q.; Gao, M.; Feng, G.; Liu, B. Mitochondria-targeted cancer therapy using a light-up probe with aggregation-induced-emission characteristics. *Angew. Chem., Int. Ed.* **2014**, *53* (51), 14225–14229.
- (26) Chen, L. B. Mitochondrial membrane potential in living cells. *Annu. Rev. Cell Biol.* **1988**, *4* (1), 155–181.
- (27) Flewelling, R. F.; Hubbell, W. L. The membrane dipole potential in a total membrane potential model. Applications to hydrophobic ion interactions with membranes. *Biophys. J.* **1986**, *49* (2), 541–52.
- (28) Honig, B. H.; Hubbell, W. L.; Flewelling, R. F. Electrostatic interactions in membranes and proteins. *Annu. Rev. Biophys. Chem.* **1986**, *15*, 163–193.
- (29) Hu, Z.; Sim, Y.; Kon, O. L.; Ng, W. H.; Ribeiro, A. J.; Ramos, M. J.; Fernandes, P. A.; Ganguly, R.; Xing, B.; Garcia, F.; Yeow, E. K. Unique Triphenylphosphonium Derivatives for Enhanced Mitochondrial Uptake and Photodynamic Therapy. *Bioconjugate Chem.* **2017**, *28* (2), 590–599.
- (30) Li, P.; Wischert, R.; Métivier, P. Mild Reduction of Phosphine Oxides with Phosphites To Access Phosphines. *Angew. Chem., Int. Ed.* **2017**, *56* (50), 15989–15992.
- (31) Culcasi, M.; Berchadsky, Y.; Gronchi, G.; Tordo, P. Anodic behavior of crowded triarylphosphines. ESR study of triarylphosphoniumyl radicals, Ar₃P⁺. *J. Org. Chem.* **1991**, *56* (11), 3537–3542.
- (32) Bruno, I. J.; Cole, J. C.; Edgington, P. R.; Kessler, M.; Macrae, C. F.; McCabe, P.; Pearson, J.; Taylor, R. New software for searching the Cambridge Structural Database and visualizing crystal structures. *Acta Crystallogr., Sect. B: Struct. Sci.* **2002**, *58* (3–1), 389–397.
- (33) Corbridge, D. E. *Phosphorus: Chemistry, Biochemistry and Technology*; CRC Press, 2016.
- (34) Winiwarter, S.; Ridderström, M.; Ungell, A. L.; Andersson, T. B.; Zamora, I. In *Comprehensive Medicinal Chemistry II*; Triggler, D. J., Ed.; Elsevier: Oxford, 2007; pp 531–554.
- (35) Ozsvári, B.; Sotgia, F.; Lisanti, M. P. Exploiting mitochondrial targeting signal(s), TPP and bis-TPP, for eradicating cancer stem cells (CSCs). *Aging* **2018**, *10* (2), 229–240.
- (36) Ketterer, B.; Neumcke, B.; Lauger, P. Transport Mechanism of Hydrophobic Ions through Lipid Bilayer Membranes. *J. Membr. Biol.* **1971**, *5* (3), 225–245.
- (37) Ross, M. F.; Kelso, G. F.; Blaikie, F. H.; James, A. M.; Cocheme, H. M.; Filipovska, A.; Da Ros, T.; Hurd, T. R.; Smith, R. A. J.; Murphy, M. P. Lipophilic triphenylphosphonium cations as tools in mitochondrial bioenergetics and free radical biology. *Biochemistry* **2005**, *44* (2), 222–230.
- (38) El Tayar, N.; Testa, B.; Carrupt, P. A. Polar intermolecular interactions encoded in partition coefficients: an indirect estimation of hydrogen-bond parameters of polyfunctional solutes. *J. Phys. Chem.* **1992**, *96* (3), 1455–1459.
- (39) Haslop, A.; Wells, L.; Gee, A.; Plisson, C.; Long, N. One-pot multi-tracer synthesis of novel (18)F-labeled PET imaging agents. *Mol. Pharmaceutics* **2014**, *11* (11), 3818–3822.
- (40) Zhang, Z.; Jenni, S.; Zhang, C.; Merckens, H.; Lau, J.; Liu, Z.; Perrin, D. M.; Benard, F.; Lin, K. S. Synthesis and evaluation of (18)F-trifluoroborate derivatives of triphenylphosphonium for myocardial perfusion imaging. *Bioorg. Med. Chem. Lett.* **2016**, *26* (7), 1675–1679.
- (41) Chen, S.; Zhao, Z.; Zhang, Y.; Fang, W.; Lu, J.; Zhang, X. Effect of methoxy group position on biological properties of (18)F-labeled benzyl triphenylphosphonium cations. *Nucl. Med. Biol.* **2017**, *49*, 16–23.
- (42) While increased molecular radius from additional methyl groups can be approximated from the molecular volume (assuming a hypothetical sphere of the same volume), this approach is incapable of reproducing the effect of adding individual methyl groups on a nonspherical molecular scaffold.
- (43) Ghanty, T. K.; Ghosh, S. K. Correlation between Hardness, Polarizability, and Size of Atoms, Molecules, and Clusters. *J. Phys. Chem.* **1993**, *97* (19), 4951–4953.
- (44) Horobin, R. W. In *Mitochondrial Medicine: Vol. II, Manipulating Mitochondrial Function*; Weissig, V., Edeas, M., Ed.; Springer: New York, NY, 2015; pp 13–23.
- (45) Horobin, R. W.; Rashid-Doubell, F.; Pediani, J. D.; Milligan, G. Predicting small molecule fluorescent probe localization in living cells using QSAR modeling. 1. Overview and models for probes of structure, properties and function in single cells. *Biotech. Histochem.* **2013**, *88* (8), 440–460.
- (46) Horobin, R. W.; Rashid-Doubell, F. Predicting small molecule fluorescent probe localization in living cells using QSAR modeling. 2. Specifying probe, protocol and cell factors; selecting QSAR models; predicting entry and localization. *Biotech. Histochem.* **2013**, *88* (8), 461–476.